

# Ferromagnetic coupling and magnetic anisotropy in molecular Ni(II) squares

R. Koch, O. Waldmann, and P. Müller

*Physikalisches Institut III, Universität Erlangen-Nürnberg, D-91058 Erlangen, Germany*

U. Reimann and R. W. Saalfrank

*Institut für Organische Chemie, Universität Erlangen-Nürnberg, D-91054 Erlangen, Germany*

(Dated: March 22, 2022)

We investigated the magnetic properties of two isostructural Ni(II) metal complexes  $[\text{Ni}_4\text{L}_8^b]$  and  $[\text{Ni}_4\text{L}_8^c]$ . In each molecule the four Ni(II) centers form almost perfect regular squares. Magnetic coupling and anisotropy of single crystals were examined by magnetization measurements and in particular by high-field torque magnetometry at low temperatures. The data were analyzed in terms of an effective spin Hamiltonian appropriate for Ni(II) centers. For both compounds, we found a weak intramolecular ferromagnetic coupling of the four Ni(II) spins and sizable single-ion anisotropies of the easy-axis type. The coupling strengths are roughly identical for both compounds, whereas the zero-field-splitting parameters are significantly different. Possible reasons for this observation are discussed.

PACS numbers: 33.15.Kr, 71.70.-d, 75.10.Jm, 75.30.Et,

## I. INTRODUCTION

Modern inorganic chemistry provides arrangements of magnetic metal ions in highly symmetric geometries, where the metal centers are separated by organic ligands. Compounds with a topologically simple arrangement of their metal centers like grids and rings have been investigated extensively. [1, 2, 3, 4, 5, 6] Due to their high symmetry it is possible to experimentally determine the magnetic parameters of large and rather complex systems. As intermolecular effects are negligible in these systems, they actually form perfect models to explore finite size spin systems. [7] In a number of cases, several related species of a compound class are available, allowing to observe correlations between crystallographic structure and magnetic properties. [6, 8] Investigation of such correlations is of key help for understanding e.g. coupling mechanisms in detail. [9]

Recently, the highly symmetric Ni(II) square  $[\text{Ni}_4\text{L}_8^b]$  with  $\text{L}^b = \text{C}_5\text{H}_4\text{N-CON-CN}_4\text{-C}_2\text{H}_5$  attracted considerable interest. [10, 11] Preliminary magnetic studies of powder samples revealed a sizeable ferromagnetic coupling of the four Ni(II) metal centers within a molecule. This system is thus one of the very rare examples of a ferromagnetic Ni(II) complex. A second species,  $[\text{Ni}_4\text{L}_8^c]$  with  $\text{L}^c = \text{C}_5\text{H}_4\text{N-CSN-CN}_4\text{-C}_2\text{H}_5$ , could be also synthesized. [11, 12] The two ligands used differ only at one position, i.e the oxygen in  $\text{L}^b$  is replaced by a sulfur in  $\text{L}^c$ . Interestingly, the two  $\text{Ni}_4$  squares are not only isostructural. Their magnetically relevant geometrical dimensions actually differ by less than 3.5%. This leads to a new situation: Differences in magnetic properties stem predominately from different electronic properties of oxygen and sulfur and not from geometrical distinctions. It is the purpose of this work to investigate the magnetism, especially the magnetic coupling and anisotropy, of these two compounds in detail.

When focusing on anisotropic properties, several ex-

TABLE I: Comparison of selected distances and bonding angles of the coordination sphere for the compounds  $[\text{Ni}_4\text{L}_8^b]$  and  $[\text{Ni}_4\text{L}_8^c]$ . Considering the nickel centers at the upper right corners in Figs. 1(b) and 1(c), respectively, the N atoms of their coordination spheres were numbered clockwise from N1 to N5 starting with oxygen/sulfur.

	$[\text{Ni}_4\text{L}_8^b]$	$[\text{Ni}_4\text{L}_8^c]$
Ni - O/S	2.032(2) Å	2.051(3) Å
Ni - N1	2.081(3) Å	2.073(4) Å
Ni - N2	2.076(3) Å	2.072(4) Å
Ni - N3	2.111(3) Å	2.074(4) Å
Ni - N4	2.065(3) Å	2.112(4) Å
Ni - N5	2.062(3) Å	2.070(4) Å
O/S - Ni - N1	88.44(11) °	86.98(15) °
N1 - Ni - N2	79.02(13) °	78.04(17) °
N2 - Ni - N3	94.62(12) °	98.04(12) °
N3 - Ni - N4	79.26(11) °	79.20(15) °
N4 - Ni - N5	90.28(12) °	92.46(15) °
N5 - Ni - O/S	83.24(11) °	83.30(14) °

perimental methods like SQUID magnetometry, EPR and torque magnetometry are possible. Torque magnetometry has been proven to be a very valuable tool in this field. [2, 5, 6]

## II. EXPERIMENTAL

### A. Preparation and Crystal Structures

The tetranuclear Ni(II) cluster  $[\text{Ni}_4\text{L}_8^b] \cdot 4\text{CH}_2\text{Cl}_2$  with  $\text{L}^b = \text{C}_5\text{H}_4\text{N-CON-CN}_4\text{-C}_2\text{H}_5$  was prepared as described in Ref. 10. The isostructural compound  $[\text{Ni}_4\text{L}_8^c] \cdot 4\text{CH}_2\text{Cl}_2$  with  $\text{L}^c = \text{C}_5\text{H}_4\text{N-CSN-CN}_4\text{-C}_2\text{H}_5$  was synthesized with a method analogous to that used for the  $[\text{Ni}_4\text{L}_8^b]$  complex. [12] The two ligands  $\text{L}^b$  and  $\text{L}^c$  are

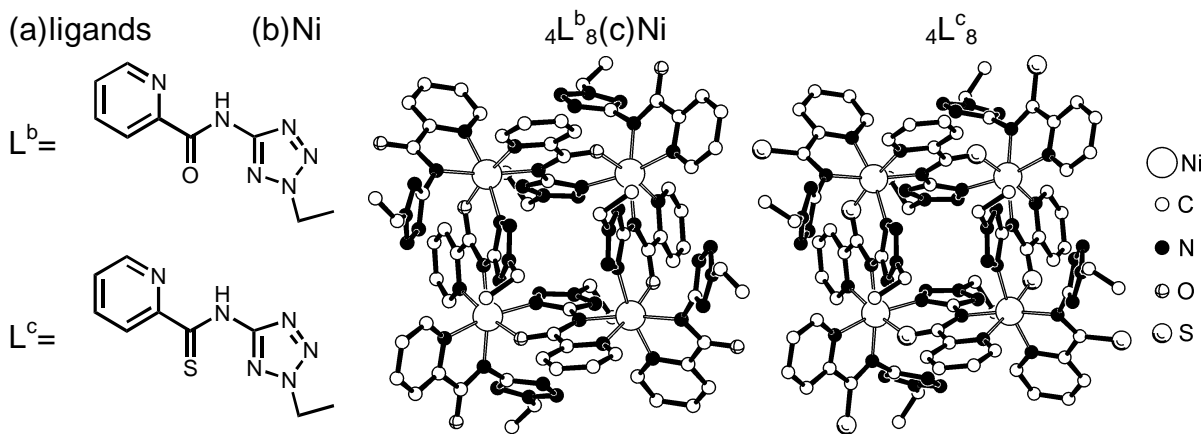


FIG. 1: (a) Sketch of both ligands  $L^b$  and  $L^c$ . (b) Structural representation of  $[Ni_4L_8^b]$  and (c)  $[Ni_4L_8^c]$  (view along the crystallographic  $S_4$ -axis, H atoms omitted).

sketched in Fig. 1. They only differ by one position: The  $C=O$  group in  $L^b$  is replaced by a  $C=S$  group in  $L^c$ .

The crystal structures were determined by X-ray structure analysis of single crystals. [10, 12] Both compounds crystallize in the space group  $I4(1)/a$ . They exhibit crystallographic  $S_4$  molecular symmetry with the four nickel centers forming almost regular squares (Fig. 1). The molecular  $S_4$  symmetry axes are perpendicular to the planes of the molecules defined by the Ni centers, and necessarily coincide with the magnetic  $z$ -axes of the molecules. The shape of the crystals is quadratic bipyramidal. The molecular magnetic  $z$ -axes are thus parallel to the  $S_4$  symmetry axis of the crystals.

The eight ligands in a molecule coordinate the nickel centers in two different ways (Fig. 1). A set of four ligands links two nickel centers each and builds up the  $[Ni_4L_4]^{4+}$  square-like cores. The second set of four ligands coordinates the nickel centers at the corners of the square cores. Each nickel center is surrounded by six donor atoms, five N and one O for  $[Ni_4L_8^b]$  and five N and one S for  $[Ni_4L_8^c]$ , respectively, forming slightly distorted octahedral coordination spheres.

Although the sulfur donors are significantly larger than the oxygen donors, the structures of the two complexes are remarkably similar. This is evident from a careful inspection of Figs. 1(b) and 1(c). The most notable structural difference arises for the  $CN_4-C_2H_5$  groups of the corner-ligands. Their orientations differ slightly in the two compounds. This is plausible since these groups are not coordinated to nickel centers.

However, the geometry of the nickel coordination sphere as well as the structure of the ligand linking two nickel ions are almost not affected by the replacement of oxygen with sulfur (Table I). The Ni-Ni next neighbor distance is  $5.567(5)$  Å for  $[Ni_4L_8^b]$  and  $5.560(5)$  Å for  $[Ni_4L_8^c]$ . Several further distances and bond angles are listed in Table I for both compounds.

These structural elements are most relevant for the magnetic properties, i.e. ligand-field and superexchange

interactions. As the two molecules are almost structurally identical, the potentially different magnetic properties of  $[Ni_4L_8^b]$  and  $[Ni_4L_8^c]$  should be controlled predominantly by the different electronic properties of oxygen and sulfur.

## B. Magnetization Measurements

For magnetization measurements, a single crystal was selected by light microscopy in the mother liquor. To avoid decomposition, the crystal was transferred directly from the solution into Apiezon grease and mounted on a plastic straw. The weight of the crystals was typically  $100 \mu\text{g}$ . The background signal of grease and sample holder was negligible compared to the signal of the crystals. Magnetic moment was measured with a MPMS-7 SQUID magnetometer from Quantum Design. The temperature range was 1.8- 300 K, the maximum magnetic field 5.5 T. The measurements were performed for magnetic fields parallel and perpendicular to the  $z$ -axis of the crystal. Due to the quadratic bipyramidal shape of the single crystals, none of the crystal planes is parallel to the magnetic  $z$ -axis. Therefore, a proper orientation of the sample on the sample holder was difficult. The orientation accuracy was about  $10^\circ$ . Two samples of each compound were investigated.

## C. Magnetic Torque Measurements

Torque measurements of single crystal samples were performed with an appropriately designed silicon cantilever torque sensor which will be described in detail in the next chapter. As for magnetization measurements, a crystal was selected from the mother liquor, immediately covered with grease, and mounted on the torque sensor. The typical sample weight was less than  $10 \mu\text{g}$ , but could be determined only within an error of 50% due to the

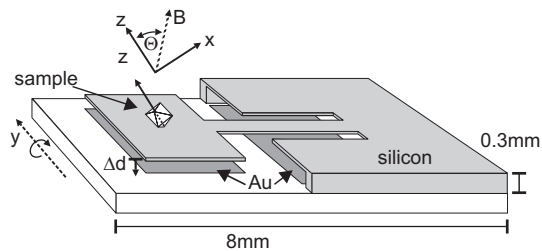


FIG. 2: Sketch of the silicon torquemeter described in section III. The typical orientation of a quadratic bipyramidally shaped crystal sample and its  $z$ -axis are shown. For adjusting the angle  $\Theta$ , the device could be rotated in-situ around the magnetic  $y$ -axis.

unknown amount of grease covering the crystals. Therefore, the number of molecules in a crystal,  $X$ , is known only roughly and a calibration of the torque signal was not feasible. The torquemeter was mounted on a rotating plate which allowed an in-situ orientation of the crystal with an accuracy of  $0.3^\circ$ . The sample was mounted on the sensor with its  $z$ -axis perpendicular to the rotation axis, as indicated in Fig. 2. The positioning accuracy was better than  $3^\circ$ , which is much better than for the magnetization measurements. Figure 2 defines the angle  $\Theta$  between magnetic field and magnetic  $z$ -axis of the crystal. The torquemeter provides a resolution of  $10^{-11}$  Nm. It was inserted into a 15/17 T superconducting cryomagnet system. The temperature was adjusted by a variable temperature insert. Typically, torque measurements versus applied magnetic field were performed at 15 different angles  $\Theta$  in a range of  $220^\circ$ . The lowest temperature was 1.8 K. For several samples, the low-field range was investigated in detail, i.e. at 60 different angles in a range of  $180^\circ$ . 5 samples of each compound were investigated.

### III. SILICON CANTILEVER TORQUEMETER

A schematic drawing of the cantilever device is presented in Fig. 2. The cantilever is mounted on a substrate of crystalline quartz glass. It is made from a very pure crystalline silicon wafer (resistivity  $> 3$  k $\Omega$ cm) with a (100) surface orientation and thickness of  $300 \mu\text{m}$ . The use of crystalline silicon guarantees excellent mechanical as well as non-magnetical properties. As shown in Fig. 2, the single crystal silicon cantilever consists of parts at the original thickness of  $300 \mu\text{m}$  and strongly thinned parts. This has been achieved by different masks on the two sides of the wafer. The masks were formed by  $1 \mu\text{m}$  thick  $\text{SiO}_2$  layers grown on both sides of the silicon wafer which were patterned by standard photolithography and etching with buffered fluorine acid. The silicon cantilever itself was etched by hot KOH to a thickness of  $10\text{-}30 \mu\text{m}$ . A  $200\text{nm}$  gold layer was evaporated on the bottom side of the cantilever. Together with gold pads structured on the quartz substrate it forms a capacitor and a reference capacitor (which is placed at the right hand section of

the device in Fig. 2). Finally, the cantilever was glued on the quartz substrate.

The torque of the sample causes a deflection of the cantilever which is detected by a change of the capacitance  $\Delta C$ . For readout, the two capacitors were connected to a ratio transformer forming an ac bridge. With this setup a sensitivity of  $\Delta C/C_0 = 10^{-7}$  is readily obtained. [13, 14]  $C_0$  denotes the zero-field capacitance (1 pF). The properties of the cantilever torquemeter can be modeled as follows: The deflection is  $\Delta d = (3/2)\tau/(D_c L_c)$ , where  $D_c$  is the spring constant and  $L_c$  the length of the cantilever. The change of the capacitance is given by  $\Delta C/C_0 \approx \Delta d/d_0(1 + \Delta d/d_0)$ , where  $d_0$  denotes the distance of the capacitor plates. This relation shows nonlinear behavior. However, for all measurements presented in this work nonlinearity was less than 2% and could be neglected. With  $U_0$  being a characteristic of the ac bridge, its output voltage can be expressed as  $U = U_0(\Delta C/C_0)$ . Altogether, one obtains  $U = K\tau(1 + \alpha K\tau)$  with the calibration constant  $K$  and the nonlinearity  $\alpha$ . If required,  $K$  and  $\alpha$  may be obtained from an explicit calibration which can be done quite easily in many ways. [14, 15, 16] As we were not able to determine the weight of the samples accurately, calibration of the device was not necessary.

### IV. THEORY

The appropriate Hamiltonian for molecular spin clusters consisting of Ni(II) centers is given by [7, 17]

$$H = - \sum_{i < j} J_{ij} \mathbf{S}_i \cdot \mathbf{S}_j + \sum_i \mathbf{S}_i \cdot \mathbf{D}_i^{\text{lig}} \cdot \mathbf{S}_i + \mu_B \sum_i \mathbf{S}_i \cdot \mathbf{g}_i \cdot \mathbf{B} \quad (1)$$

with  $\mathbf{S}_i = 1$  and the following standard terms: a Heisenberg term modeling isotropic next-neighbor exchange interactions, a zero-field-splitting (ZFS) term due to ligand-field interactions, and the Zeeman term. Due to the small coupling constants in  $[\text{Ni}_4\text{L}_8^b]$  and  $[\text{Ni}_4\text{L}_8^c]$ , anisotropic and biquadratic coupling terms can be neglected. Dipole-dipole interactions are negligible due to the large distances of the spin centers. Cross-coupling superexchange terms hardly exist as corresponding coupling paths are not present. Due to the molecular  $S_4$  symmetry of the complexes, magnetic anisotropy is strictly uniaxial and a simplified Hamiltonian is obtained:

$$H = -J \sum_{i < j} \mathbf{S}_i \cdot \mathbf{S}_j + D \sum_i (S_{i,z}^2 - 2/3) + \mu_B g_{xy} (S_x B_x + S_y B_y) + \mu_B g_z S_z B_z. \quad (2)$$

Thus, four magnetic parameters are sufficient to describe the properties of the  $\text{Ni}_4$  squares correctly: the coupling constant  $J$ , the ZFS parameter  $D$  and the two

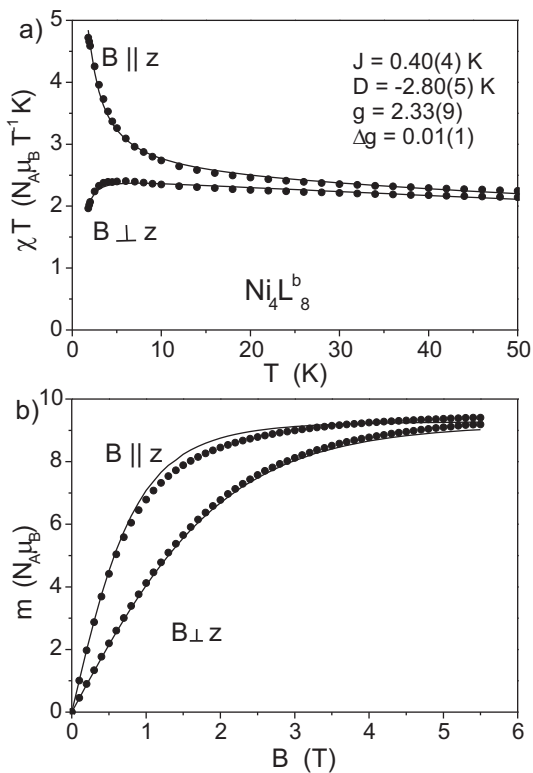


FIG. 3: (a) Magnetic susceptibility times temperature vs. temperature and (b) magnetic moment vs. magnetic field at  $T = 1.8$  K of a  $[\text{Ni}_4\text{L}_8^b]$  crystal for two different orientations of magnetic field. The solid lines represent best fits based on eq. (2).

$g$ -factors  $g_{xy}$  and  $g_z$ . In the following we will use the parameterization  $g = \sqrt{(2g_{xy}^2 + g_z^2)}/3$  and  $\Delta g = g_z - g_{xy}$  for the  $g$ -factors. As we will see,  $J \approx 0.9$  K and  $D \approx -2.5$  K. Thus neither the strong exchange limit ( $|D/J| \ll 1$ ) nor the Ising limit ( $|D/J| \gg 1$ ) is valid. Therefore, a full matrix diagonalization has to be performed. Due to the small dimension of the Hilbert space of  $3^4 = 81$ , this can be done on a commercial PC. Calculation time could be reduced by a factor of 12 by taking into account a  $C_{2v}$  spin permutational symmetry of Hamiltonian eq. (2). [18]

## V. MAGNETIZATION MEASUREMENTS: RESULTS AND ANALYSIS

Magnetic susceptibility and magnetization curves for  $[\text{Ni}_4\text{L}_8^b]$  with magnetic field parallel and perpendicular to the magnetic  $z$ -axis are shown in Fig. 3. Fits based on eq. (2) revealed the following parameters:  $J = 0.40(4)$  K,  $D = -2.80(5)$  K,  $g = 2.33(9)$  and  $\Delta g = 0.01(1)$  for  $[\text{Ni}_4\text{L}_8^b]$  and  $J = 0.40(4)$  K,  $D = -1.80(8)$  K,  $g = 2.33(9)$  and  $\Delta g = 0.01(1)$  for  $[\text{Ni}_4\text{L}_8^c]$ . It should be noted, that the given errors reflect statistical uncertainties only and do not include systematical errors. Detailed simulations

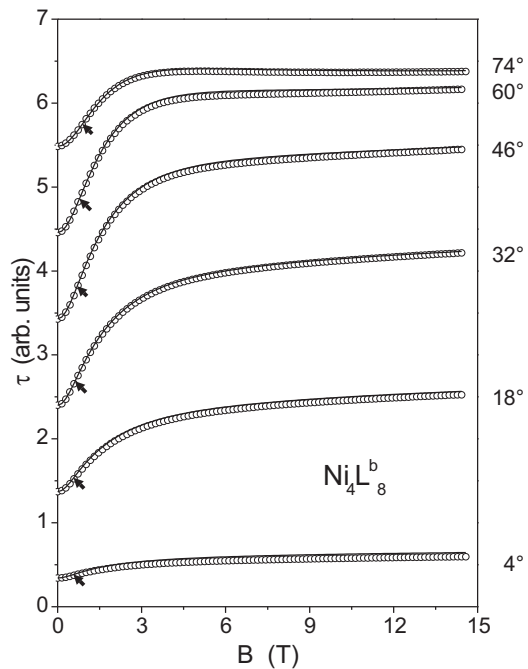


FIG. 4: Torque measurements vs. magnetic field of a  $[\text{Ni}_4\text{L}_8^b]$  crystal sample at several angles  $\Theta$  and  $T = 1.8$  K (circles). The curves are shifted for clarity. The solid lines represent fits using Hamiltonian eq. (2). The arrows indicate the inflection points of the curves.

showed that the low temperature behavior of the magnetization is very sensitive to a misalignment of the crystal. Already a misalignment of  $5^\circ$ , which is well within experimental uncertainty (see section II B), leads to notably different parameters. Therefore, the results from the magnetization measurements will be regarded as guidelines and will not be discussed further. Nevertheless, a trend is indicated: The coupling constants are roughly identical in both compounds, whereas the ZFS parameters differ significantly.

## VI. TORQUE MAGNETOMETRY: RESULTS AND ANALYSIS

The torque measurements were analyzed by fitting Hamiltonian eq. (2) to the data. As the torque signal was uncalibrated, the number  $X$  of molecules in a sample had to be considered also as a free parameter, in addition to the parameters  $J$ ,  $D$ ,  $g$ , and  $\Delta g$ . In our first attempt to determine the magnetic parameters, we fitted the complete angular dependence  $\tau(B, \Theta)$  of a sample with  $X$ ,  $J$ ,  $D$  and  $\Delta g$  varying simultaneously.  $g$  was fixed to reasonable values between 2.1 and 2.3. [7, 19, 20] A typical data set with corresponding fit is shown in Fig. 4. Concerning the parameter  $R = \sum (\tau_{sim} - \tau_{meas})^2 / \sum \tau_{meas}^2$ , which estimates the quality of the least square fits, we obtained excellent results. Unfortunately, this approach revealed rather large variations of the parameters for different

TABLE II: Magnetic parameters for the examined molecules.

	$J$ (K)	$D$ (K)	$\Delta g$
$[\text{Ni}_4\text{L}_8^b]$	0.9(1)	-2.7(1)	0.01(1)
$[\text{Ni}_4\text{L}_8^c]$	0.9(1)	-2.0(1)	0.01(1)

samples. However, fixing one additional parameter besides  $g$  yielded stable fitting results. Thus, either  $J$ ,  $D$  or  $\Delta g$  should be determined in a different way. As we will show, this can be done without additional experimental data. The improved strategy rests on the fact, that a fit to the whole data set does not consider that the parameters affect individual parts of the torque curves selectively. A careful study of numerical simulations based on Hamiltonian eq. (2) provides valuable information concerning this topic.

Figure 3(b) shows that the magnetization curves saturate at fields of about 5 T. This is easily understood as calculations show that the ground state is well separated from the excited states at 5 T ( $\Delta E > 5$  K). The torque measurements exhibit similar saturation (Fig. 4). In this field regime, the torque curves are featureless and the magnitude is controlled by  $X$ ,  $\Delta g$ , and  $D$  simultaneously. Here the curves are over parameterized.

For a detailed examination of the low-field part, it is useful to analyze the behavior of the inflection points  $B_{ip}(\Theta)$  of the torque curves. In this way, the parameter  $X$  is eliminated as the value of  $B_{ip}(\Theta)$  is independent of the magnitude of the curves. Figure 4 shows that the inflection points vary slightly with  $\Theta$ . The calculated angular dependence of  $B_{ip}$  for different values of  $J$  and  $D$  is presented in Fig. 5. It turns out that the offset of the oscillation is shifted downwards with increasing  $J$  (and  $g$ , not shown here). On the other hand, the offset is not influenced by  $D$  and, as further simulations showed, by  $\Delta g$ . In contrast, the amplitude of the oscillation is controlled by  $D$  exclusively. So it is possible to extract the values of  $D$  and  $J$  (for given  $g$ ) from analyzing the inflection points of the measured torque curves. As  $g$  should be between 2.1 and 2.3,  $J$  may be obtained with an accuracy of 10%.

For two samples of every compound, we determined  $B_{ip}(\Theta)$  from measurements at 60 different angles. Fitting this data (Fig. 6) revealed  $D$  and  $J$  very precisely. To obtain the remaining parameter  $\Delta g$ , the whole torque data set  $\tau(B, \Theta)$  was fitted with  $D$  and  $g$  fixed. As  $J$  was not fixed in this procedure, it could be determined again and compared to the value extracted from  $B_{ip}(\Theta)$ . This provided prove for the consistency of our analysis. The parameters for the two compounds are summarized in Table II.

## VII. DISCUSSION

The value of  $J$  observed for powder samples of  $[\text{Ni}_4\text{L}_8^b]$  in Ref. 10 is almost a factor of two larger than that deter-

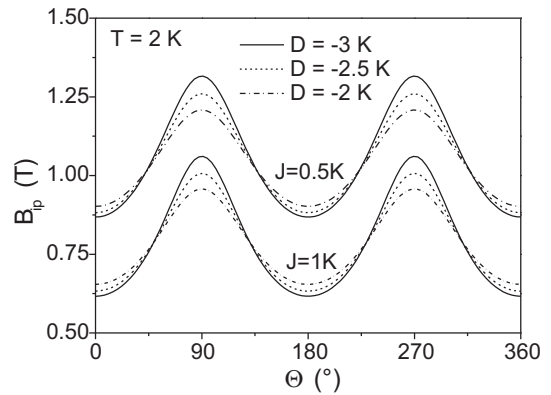


FIG. 5: Calculated values for the inflection point  $B_{ip}$  of torque curves as function of  $\Theta$  for different parameters  $J$  and  $D$  ( $g = 2.2$ ,  $\Delta g = 0$ ).

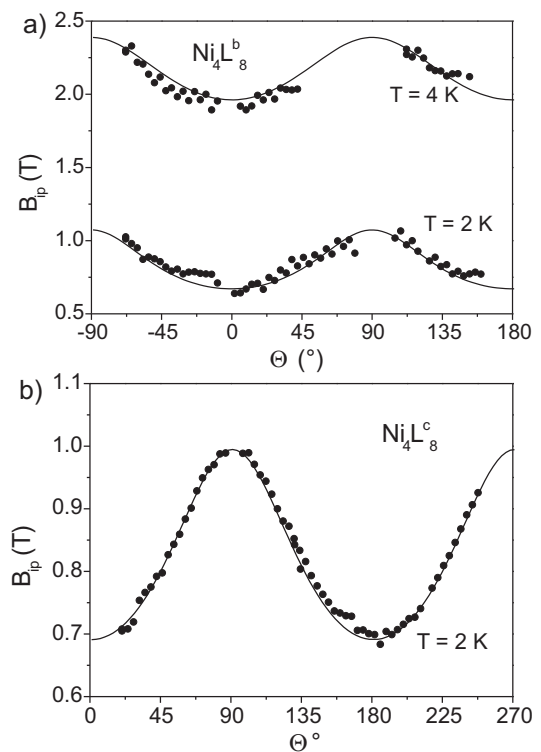


FIG. 6:  $B_{ip}$  vs. angle  $\Theta$  of measured torque curves for (a)  $[\text{Ni}_4\text{L}_8^b]$  and (b)  $[\text{Ni}_4\text{L}_8^c]$ . Solid lines represent fits using eq. (2). For  $[\text{Ni}_4\text{L}_8^b]$ , data sets for two temperatures have been used simultaneously in the analysis.

mined here. We ascribe this to structural changes of the cluster resulting from loss of  $\text{CH}_2\text{Cl}_2$  molecules upon drying of crystals. This effect has been observed for other molecules, which decompose rapidly under exposure to air, too. [6, 16] The different values for  $J$  obtained from single crystal SQUID measurements as compared to the torque results is explained by misalignment errors as discussed in section V.

Within the error ranges, the value of  $\Delta g$  is consistent

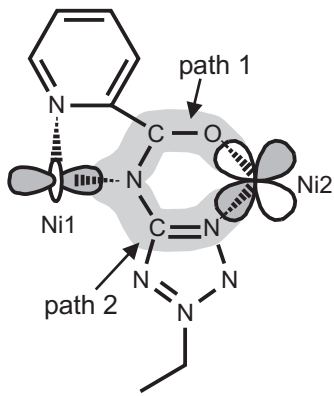


FIG. 7: Sketch of the ligand  $L_8^b$  bridging two nickel ions, the free metal orbitals of the two linked Ni centers, and the two obvious coupling paths.

with predictions of ligand-field theory: From  $\Delta g = 2D/\lambda$  and  $\lambda = -250$  K appropriate for Ni(II) centers [19] one obtains  $\Delta g = 0.02$ .

The above analysis demonstrated that the coupling constants are identical within experimental accuracy in both compounds, whereas the ZFS parameters differ significantly. The geometry of the Ni coordination spheres are essentially identical for the two complexes. Thus, different values of  $D$  should be ascribed to different electronic environments of the Ni centers. In particular, the different donor capabilities of oxygen and sulfur should clearly affect the ligand-fields and thus the ZFS parameters.

The results for  $J$  are more puzzling. The special geometrical arrangement of the two coordination pockets leads to an orthogonality of the metal orbitals. To point this out, Fig. 7 shows a sketch of the ligand  $L^b$  linking two Ni centers and the relevant metal orbitals (hypothetical orbitals of a free Ni atom). The magnetic orbitals should extend along the coupling path between neighboring Ni ions as indicated by the gray background in Fig. 7. The coupling path actually may be split in two sub-paths, path 1 along the Ni-N-C-O-Ni chain and path 2 along the Ni-N-C-N-Ni chain. This suggests an explanation for the observed ferromagnetic couplings: When path 1 and path 2 contribute equally to the magnetic coupling, the overlap of the magnetic orbitals will be zero for parity reasons. Then, magnetic coupling would be ferromagnetic since an antiferromagnetic contribution, which is proportional to the overlap, cancels out. [21]

However, path 1 of the coupling path is quite differ-

ent for  $[\text{Ni}_4L_8^b]$  and  $[\text{Ni}_4L_8^c]$ , as demonstrated by the observed different values for  $D$ . Thus, one would expect that also the coupling constants are clearly different, in contrast to experimental observation. This suggests that the magnetic coupling is predominantly controlled by path 2. But then, an antiferromagnetic coupling should be expected which generally dominates if the overlap is non-zero. [21] Obviously, the ferromagnetic coupling in  $[\text{Ni}_4L_8^b]$  and  $[\text{Ni}_4L_8^c]$  is the result of a subtle balance between ferromagnetic and antiferromagnetic contributions which is not easily reconciled with present knowledge.

## VIII. CONCLUSION

The two  $\text{Ni}_4$  compounds studied in this work are of interest for three reasons: (i) Ferromagnetic coupling in molecular spin systems is rather rare. Concerning polynuclear Ni complexes, only few systems are known to date. [22] (ii) The high crystallographic symmetry reduces the number of magnetic parameters significantly, allowing very accurate determination of the magnetic parameters. (iii) Two species with minimal geometrical differences of one system facilitates an isolation of possible links between ligand-field splitting or magnetic coupling, respectively, and electro-structural properties.

We showed that  $J$  and  $D$  can be determined very accurately by torque magnetometry in combination with sophisticated analysis also for systems where  $J$  and  $D$  are on the same order of magnitude. This extends recent applications of torque magnetometry to molecular nanomagnets. [2, 5, 6]

The differences of the anisotropy parameter  $D$  have been ascribed to local differences in the electronic environment of the Ni centers. For the coupling constant  $J$  some mechanisms have been suggested but no final explanation could be given. Ab-initio calculations would be of great help to provide comprehensive explanations for the origin and the strength of the coupling. [23]

## Acknowledgments

We would like to thank Andreas Richter for help in the lab and Jochen Thomas for silicon handling. Furthermore we thank Stefan Schromm and Stephan Rother for valuable discussions. This work was supported by the Deutsche Forschungsgemeinschaft.

- 
- [1] O. Waldmann, J. Hassmann, P. Müller, G. S. Hanan, D. Volkmer, U. S. Schubert, and J.-M. Lehn, *Phys. Rev. Lett.* **78**, 3390 (1997).  
 [2] O. Waldmann, R. Koch, S. Schromm, P. Müller, L. Zhao, and L. K. Thompson, *Chem. Phys. Lett.* **332**, 73 (2000).  
 [3] O. Waldmann, L. Zhao, and L. K. Thompson, *Phys. Rev.*

- Lett.* **88**, 066401 (2002).  
 [4] K. L. Taft, C. D. Delfs, G. C. Papaefthymiou, S. Foner, D. Gatteschi, and S. J. Lippard, *J. Am. Chem. Soc.* **116**, 823 (1994).  
 [5] A. Cornia, M. Affronte, A. G. M. Jansen, G. L. Abbati, and D. Gatteschi, *Angew. Chem.* **111**, 2409 (1999).

- [6] O. Waldmann, R. Koch, S. Schromm, J. Schülein, P. Müller, I. Bernt, R. W. Saalfrank, F. Hampel, and E. Balthes, *Inorg. Chem.* **40**, 2986 (2001).
- [7] O. Waldmann, J. Hassmann, P. Müller, D. Volkmer, U. S. Schubert, and J.-M. Lehn, *Phys. Rev. B* **58**, 3277 (1998).
- [8] A.-L. Barra, F. Bencini, A. Caneschi, D. Gatteschi, C. Paulsen, C. Sangregorio, R. Sessoli, and L. Sorace, *Chem. Phys. Chem.* **2**, 523 (2001).
- [9] O. Kahn, *Angew. Chem.* **97**, 837 (1985).
- [10] R. W. Saalfrank, S. Trummer, U. Reimann, M. Chowdhry, F. Hampel, and O. Waldmann, *Angew. Chem. Int. Ed.* **39**, 3492 (2000).
- [11] R. W. Saalfrank, U. Reimann, F. Hampel, C. Goebel, and R. Herbst-Irmer, *Z. Naturforsch.* **57 b** (2002).
- [12] U. Reimann, *Polynukleare Metallchelatekomplexe mit verschiedenen Heterocyclen als Liganden: Synthese, Struktur und Eigenschaften* (Universität Erlangen Nürnberg, 2001).
- [13] R. C. Richardson and E. N. Smith, *Experimental Techniques in Condensed Matter Physics at low Temperatures* (Publishing Company, Inc., California, 1988).
- [14] O. Waldmann, F. Steinmayer, P. Müller, J. J. Neumeier, F. X. Regi, H. Savary, and J. Schneck, *Phys. Rev. B* **53**, 11825 (1996).
- [15] M. P. Schwarz, D. Grundler, L. Meinel, C. Heyn, and D. Heitmann, *Appl. Phys. Lett.* **76**, 3564 (2000).
- [16] O. Waldmann, J. Schülein, R. Koch, P. Müller, I. Bernt, R. W. Saalfrank, H. P. Andres, H. U. Güdel, and P. Al-lenspach, *Inorg. Chem.* **38**, 5879 (1999).
- [17] A. Bencini and D. Gatteschi, *Electron Paramagnetic Resonance of exchange coupled systems* (Springer, Berlin, 1990).
- [18] O. Waldmann, *Phys. Rev. B* **61**, 6138 (2000).
- [19] A. Abragam and M. H. L. Pryce, *Electron Paramagnetic Resonance of Transition Ions* (Clarendon Press, Oxford, 1970).
- [20] R. G. Hicks, M. T. Lemaire, L. K. Thompson, and Z. Xu, *Chem. Commun. Advance Article* (2002).
- [21] O. Kahn, *Molecular Magnetism* (VCH Publishers Inc., New York, 1993).
- [22] B. Kersting, G. Steinfeld, and D. Siebert, *Chem. Eur. J.* **19**, 4253 (2001).
- [23] J. Kortus, C. S. Hellberg, and M. R. Pederson, *Phys. Rev. Lett.* **86**, 3400 (2001).